A Novel Two-Step Scheme Based on Joint GO-DPCA and Local STAP in Image Domain for Multichannel SAR-GMTI

Zhihao Wang , *Student Member, IEEE*, Yongliang Wang, *Member, IEEE*, Mengdao Xing , *Fellow, IEEE*, Guang-Cai Sun , *Senior Member, IEEE*, Shuangxi Zhang, *Member, IEEE*, and Jixiang Xiang , *Student Member, IEEE*

Abstract—Multichannel synthetic aperture radar ground moving target indication has been widely used and get great attention nowadays. Traditional adaptive methods like space-time adaptive processing (STAP) need to calculate and search the maximum of the test statistic pixel by pixel over a large range of radial velocity, which will cause great computational burden. Nonadaptive methods like displaced phase center antenna (DPCA) will cause signal loss of moving targets, thereby degrading the performance of moving targets detection and radial velocity estimation. To improve the problem mentioned above, this article proposes a novel two-step scheme based on greatest of (GO)-DPCA and Local STAP. In step I, GO-DPCA utilizes the complex images of the channels with different baselines for joint moving target detection. Then, in step II, only the local data of moving targets detected in step I needs to be extracted from the original image domain for clutter suppression and radial velocity estimation simultaneously by STAP. Since the processing gain of moving targets depends on the radial velocity and baseline length, the detection performance of moving targets with different radial velocity can be improved by proposed GO-DPCA compared to conventional DPCA. Considering the moving targets usually distribute sparsely in the scene, step II can avoid most computational burden caused by processing pixel by pixel. Finally, the experimental results of both simulated and acquired data are given to validate the effectiveness of the proposed method.

Index Terms—Greatest of displaced phase center antenna (GO-DPCA), ground moving target indication (GMTI), space-time adaptive processing (STAP), synthetic aperture radar (SAR).

I. INTRODUCTION

MULTICHANNEL synthetic aperture radar ground moving target indication (SAR-GMTI) systems, the combination of multichannel SAR [1]–[8] and GMTI, can realize high resolution imaging for stationary objects and detection for moving targets simultaneously, which have attracted more interests and been widely used in battle reconnaissance, maritime observation [9], [10], traffic monitor [11] and other fields. In practical application, two main problems affect the performance. First, since the moving target is usually covered by the clutter, it's hard to recognize the moving target in the original SAR image. Thus, we need to perform clutter suppression before detection. Second, the radial velocity of the moving target will cause additional Doppler frequency and the displacement in azimuth. As a result, the accurate estimation of the radial velocity proves essential in relocating the moving target back to its true position in azimuth.

For the purpose of clutter suppression and radial velocity estimation, the adaptive methods [12]–[19] have been proposed. Space-time adaptive processing (STAP) [12], [13] is a typical method of them, which can suppress clutter by minimizing the power of the output clutter and making the power of moving target keep constant. STAP has been widely used in surveillance radar systems at first [14] and then applied to multichannel SAR. Ender has proposed post Doppler-STAP into post-Doppler STAP (PD-STAP) [15], which is performed in range-Doppler domain. Cerutti–Maori and Sikaneta *et al.* have derived the generalized likelihood ratio test (GLRT) statistics in the range image-azimuth signal domain and proposed imaging STAP (ISTAP) [16]–[18]. After that, they have also derived the GLRT statistics in the two-dimensional (2-D) image domain and proposed extended displaced phase center antenna (EDPCA) [19]. ISTAP and EDPCA can improve signal to noise ratio compared to PD-STAP, which is beneficial for clutter suppression. The adaptive methods are optimum and have good theoretical performance. However, their computational burdens are too expensive, which are caused by two main problems. On the one hand, the positions of moving targets are unknown at first. Thus, we need to calculate the covariance matrix and search the maximum of the test statistic pixel by pixel. Since a SAR image usually has large number of pixels, calculating and searching pixel by pixel is computational heavily. On the other hand, we can get the maximum of the test statistics only if the search value is matched with the true radial velocity of moving targets. Since the radial velocity of moving targets are unknown and each moving target has different radial velocity. In each pixel, we need to search

over a large range of radial velocity to make sure that all the possible moving targets can be detected, which will cause great computational burden as well.

On the contrary, the nonadaptive methods [20]–[26] have much smaller computational burden than the adaptive methods. Along-track interferometry (ATI) [20], [21] analyzes the statistical model of the magnitude and phase in the SAR interferogram and then derived the test statistic for moving targets detection. Displaced phase center antenna (DPCA) [22], [23], such as subspace projection (SP) [22] and images differential (ID) [23], utilizes the special antenna configuration and the images from different channels to suppress clutter. ATI and DPCA are two typical methods of the nonadaptive methods, which are used in the dual channels SAR at first and then extended to the multichannel SAR [24]–[26]. ID-ATI [24], [25] utilizes the images from adjacent channels to suppress clutter at first and then uses ATI to estimate the radial velocity of moving targets. SP-ATI [26] utilizes SP for clutter suppression and then utilizes ATI for radial velocity estimation. Nevertheless, the main problem of the nonadaptive methods is the signal loss of moving targets in the postsuppression domain. The signal loss will degrade the performance of clutter suppression and radial velocity estimation.

Just as the analysis above, the adaptive methods can realize GMTI with better theoretical performance while their computational burdens are heavy. The nonadaptive methods can be realized much faster while the signal loss will degrade their performance. In this article, our purpose is to propose an efficient method whose performance can be close to the adaptive methods while lots of computational burdens can be avoided in the practical application just like the dimensionality reduction method of the early warning radar [12]–[14]. After the analysis of existing methods, we found that the advantages of adaptive and nonadaptive methods can be used to make up the shortcomings of each other. In step I, if we use nonadaptive methods for moving targets detection, we can find the positions of moving targets in a fast way to avoid the calculation and search pixel by pixel. Then, in step II, we can use local adaptive process to get more precise results compared to step I. To the best of the authors knowledge, the current methods realize GMTI by either adaptive methods or nonadaptive methods independently. The main contribution and difference of this article is the proposed joint two-step scheme which has organic combination of nonadaptive and adaptive methods compared to existing methods. Besides, the proposed joint two-step scheme is not just the simple cascade of the current nonadaptive methods and adaptive methods. When we design our scheme, there are some problems which may degrade the performance. We have also given respective solutions to improve the proposed joint scheme. First, in step I, when we try to use a fast way to detect the positions of potential moving targets, we are concerned about the massive detection missings as the performance of nonadaptive methods may not be as good as that of adaptive methods. Therefore, we have derived the processing gain of the conventional DPCA and proposed the modified GO-DPCA. What's more, we have derived the relationship between probability of detection (PD), probability
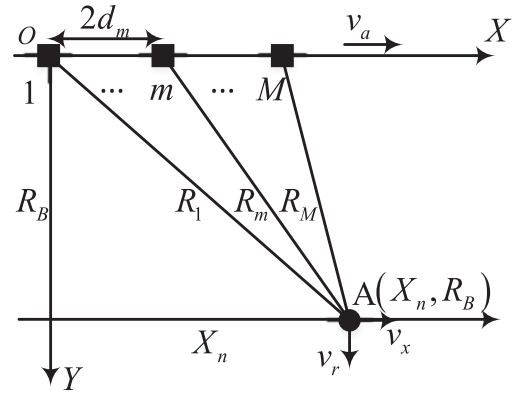

Fig. 1. Multichannel SAR-GMTI geometry model.

of false alarm (PFA) and the detection threshold. Then according to the relationship, we can decrease the threshold to improve PD and decrease detection missings. Second, in Step II, the decrease of threshold may lead to more false alarms. Therefore, we have used the output data of local adaptive process to perform moving targets detection with a normal threshold again to eliminate the supernumerary false alarms and decrease PFA.

The rest of this article is organized as follows. Section II describes the signal model of multichannel SAR-GMTI. Section III derives the processing gain of conventional DPCA and introduces the proposed two-step scheme. Section IV shows the experimental results of both simulated and acquired data and the further discussion. Eventually, a brief conclusion is presented in Section V.

II. Signal Model of Multichannel SAR-GMTI

Fig. 1 shows the geometry model of a multichannel SAR-GMTI system. The X-axis denotes the flight path of the platform whose velocity is v_a. The Y-axis denotes the radial direction which is perpendicular to the direction of the flight path. The antenna array has M channels and distributes along the direction of the flight path. The first channel is supposed to locate at the original point and seen as the reference channel. The physical interval between two adjacent channels is denoted by $2d_0$. Then the physical interval between the mth channel and the reference channel is $2d_m = 2(m-1)d_0$. According to the effective phase center model, the interval of the effective phase center between the mth channel and the reference channel are d_m. The moving target is denoted by $A(X_n, R_B)$. Its azimuth and radial velocity are v_x and v_r respectively. The slope distance between the moving target and the mth channel can be expressed as

$$R_m(t_a) = \sqrt{(R_B + v_r t_a)^2 + (X_n + v_x t_a - v_a t_a - d_m)^2}$$
$$\approx \frac{(v_a - v_x)^2}{2R_B}t_a^2 + \left(v_r - \frac{(v_a - v_x)(X_n - d_m)}{R_B}\right)t_a$$
$$+ R_B + \frac{(X_n - d_m)^2}{2R_B} \tag{1}$$

where t_a denotes the slow time in azimuth. Taylor expansion is utilized here to make a reasonable approximation. After range compression, the echo of the mth channel in 2-D time domain is expressed as

$$S_m (t_r, t_a) = \mu \cdot \mathrm{sinc} \left\{ B \left[\hat{t} - \frac{2R_m (t_m)}{c} \right] \right\} \cdot W_a (t_a)$$
$$\cdot \exp \left\{ -j \frac{4\pi}{\lambda} R_m (t_m) \right\} \tag{2}$$

where μ denotes the amplitude of echo signal. t_r denotes the fast time. B, c, and λ denote bandwidth, light speed and the wavelength, respectively, $\mathrm{sinc}(\cdot)$ is the sinc function while $W_a(\cdot)$ represents the azimuth time window function. Then, after time delay compensation and channel equalization [27], [28], the echo of the mth channel in phase-history domain is formulated as

$$S_m \left(f_r, t_a - \frac{d_m}{v_a} \right) = \mu \cdot W_r (f_r) \cdot W_a \left(t_a - \frac{d_m}{v_a} \right)$$
$$\cdot \exp \left(-j \frac{4\pi (f_r + f_c)}{c} \frac{(v_a - v_x)^2}{2R_B} t_a^2 \right)$$
$$\cdot \exp \left(-j \frac{4\pi (f_r + f_c)}{c} \left(\left(v_r - \frac{(v_a - v_x) X_n}{R_B} \right) t_a + R_{res} \right) \right) \tag{3}$$

where $W_r(\cdot)$ denotes the window function in range-frequency domain. f_c is carrier frequency and f_r is range frequency. Assuming that $v_a \gg v_x$, then the residual constant term is expressed as

$$R_{res} = R_B + \frac{X_n^2}{2R_B} - v_r \frac{d_m}{v_a}. \tag{4}$$

As shown in the last phase term of (3), the radial velocity of the moving target is coupled with the azimuth time. The coupling will cause the range walk for the moving target. Besides, v_r will also cause the displacement of the frequency spectrum in azimuth. The displacement will cause the azimuth ghost. To correct the range walk and remove azimuth ghost caused by radial velocity, the Deramp–Keystone process (DKP) [29] algorithm is used here. Then the final focusing result in 2-D image domain is expressed as

$$S_m (t_r, f_a) = \mu \cdot \mathrm{sinc} \left(B \left(t_r - \frac{2R_B}{c} \right) \right)$$
$$\cdot \mathrm{sinc} \left(T_a \left(f_a - \frac{2}{\lambda} \left(\frac{(v_a - v_x) X_n}{R_B} - v_r \right) \right) \right)$$
$$\cdot \exp \left(-j \frac{4\pi}{\lambda} \left(R_B + \frac{X_n^2}{2R_B} \right) \right) \cdot \exp \left(j \frac{4\pi}{\lambda} v_r \frac{d_m}{v_a} \right) \tag{5}$$

where T_a is synthetic aperture time. f_a represents the azimuth frequency. From (5), the steering vector in image domain for clutter and moving targets can be formulated, repectively, as [26], [30]–[31]

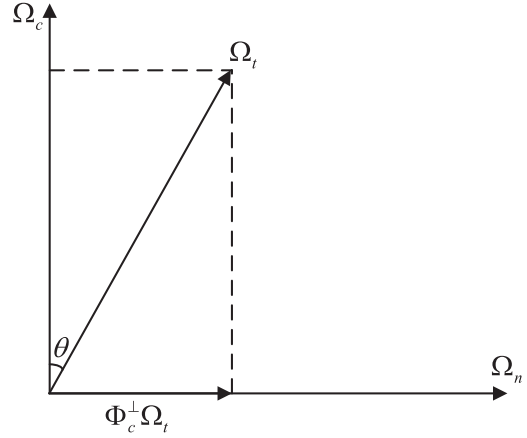$$a_c = [1, 1, \ldots, 1]^T \tag{6}$$

Fig. 2. Relationships of each subspace for projection.

$$a_t = \left[1, \ldots, \exp \left(j \frac{4\pi}{\lambda} v_r \frac{d_m}{v_a} \right), \ldots, \exp \left(j \frac{4\pi}{\lambda} v_r \frac{d_M}{v_a} \right) \right]^T. \tag{7}$$

III. IMPROVED TWO-STEP SCHEME

A. Theoretical Processing Gain of Moving Targets By DPCA

In this part, the processing gain of moving targets obtained by SP and ID are derived. First, we consider the case of SP. As shown in Fig. 2, Ω_n and Ω_c denote the noise subspace and the clutter subspace, respectively. They are orthogonal. The target subspace Ω_t and the clutter subspace Ω_c are not orthogonal. The included angle of Ω_t and Ω_c, which relies on the radial velocity of moving targets, can be expressed as

$$\theta = \arccos \frac{|\langle a_c, a_t \rangle|}{\|a_c\|_2 \cdot \|a_t\|_2} \tag{8}$$

where $\langle \cdot \rangle$ is inner product. $|\cdot|$ and $\| \cdot \|_2$ denote absolute value and $L2$ norm, respectively. We use the projection matrix, which is formulated as (9) [32], to project the echo into $\Omega_c^\perp$

$$\Phi_c^\perp = \Psi - a_c (a_c^H \cdot a_c)^{-1} a_c^H \tag{9}$$

where Ψ is the identity matrix. $[\cdot]^{-1}$ and $[\cdot]^H$ denote the inverse and conjugate transpose of the matrix, respectively. The processing gain of the clutter is zero because of the orthogonality. The processing gain of moving targets for the mth channel can be expressed as

$$\Theta_m = \Phi_c^\perp \cdot a_t (m)$$
$$= \left| \exp \left(j \frac{4\pi}{\lambda} v_r \frac{d_m}{v_a} \right) - \frac{1}{M} \sum_{u=1}^{M} \exp \left(j \frac{4\pi}{\lambda} v_r \frac{d_u}{v_a} \right) \right|,$$
$$m = 1 \sim M. \tag{10}$$

Then, the processing gain of moving targets obtained from ID is derived here. After time delay compensation and channel equalization, the differential between the complex image of the mth channel and that of the reference channel are performed. According to (5), the processing gain of moving targets can be

TABLE I
MAIN PARAMETERS OF SIMULATED DATA

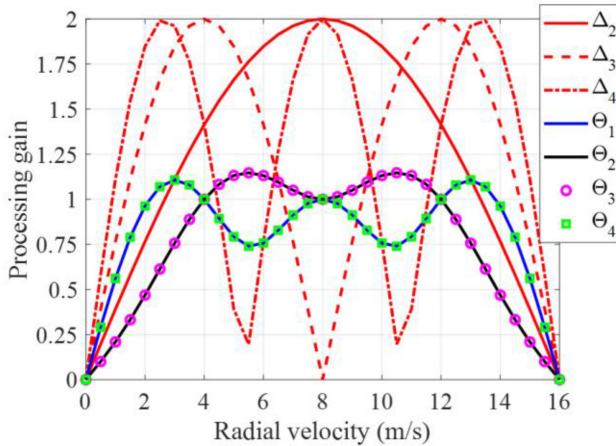| Parameter	Value
Bandwidth	30MHz
Slant range	40km
Array spacing	0.5m
Channel number	4
Platform velocity	120m/s
Carrier frequency	4.5GHz
Pulse repetition frequency	1000Hz

Fig. 3. Theoretical gain curves of moving targets by conventional DPCA.

represented as

$$\Delta_m = \frac{|S_{m1}(t_r, f_a)|}{|S_1(t_r, f_a)|}$$

$$= \frac{|S_m(t_r, f_a) - S_1(t_r, f_a)|}{|S_1(t_r, f_a)|}$$

$$= \left| 1 - \exp\left(j\frac{4\pi}{\lambda} v_r \frac{d_m}{v_a} \right) \right|, m = 2 \sim M. \quad (11)$$

From (10) and (11), we can see that the theoretical processing gain of moving targets varies with the change of the radial velocity and baseline length. We plot the processing gain curves in a single period of the radial velocity when using different values of baseline length. The other parameters are given in Table I and the results are shown in Fig. 3. Obviously, in terms of the conventional DPCA, a single value of the baseline length cannot make sure that all the moving targets with different radial velocity get their highest processing gain. For example, a moving target with $v_r = 1$m/s can obtained its highest processing gain by Δ_4 while a moving target with $v_r = 6$m/s can obtained its highest processing gain by Δ_2.

B. Step I : GO-DPCA for Joint Clutter Suppression and the Detection of Moving Targets' Positions

When we use conventional DPCA in multichannel case, M-1 times of DPCA can be applied to the second-Mth image with respect to the first image. Here we will face two problems just

as the derivation and analysis in last part. First, which data should we select to perform constant false alarm rate (CFAR). If the results of M-1 times' DPCA are all used for CFAR, we need to perform M-1 times' CFAR, which will increase the computational burdens. Second, Considering that the results of M-1 times' DPCA are different with each other, how to determine the final detection results based on different results of M-1 times' DPCA for better detection performance. A common solution which is used in [24], [25], and [41] is to utilize the image from the adjacent channels for differential. Because of the specific phase relationship which is needed for further ATI process to estimate radial velocity, this solution cannot utilize the whole baseline to make the moving targets with different radial velocity all get their highest gain. Aiming at the two problems above, we have given our solution in step I to improve the conventional DPCA. Just as shown in Fig. 4(a) which takes the example of the quad-channel, we use the maximum of $S_{21}(p_t, q_t)$, $S_{31}(p_t, q_t)$ and $S_{41}(p_t, q_t)$ as the power of the pixel under detection when detecting the pixel (p_t, q_t). For each background pixel which can be generally denoted by (p, q), we use the mean value of $S_{21}(p, q)$, $S_{31}(p, q)$ and $S_{41}(p, q)$ as their power. Then the values of these two kinds of pixels are utilized in the final CFAR detection jointly. In this way, we only need to perform one time of CFAR. What's more, assume that a local region only contains one moving target with a constant radial velocity, then the moving targets with different radial velocity can always get their highest processing gain compared to the conventional DPCA. The processing gain curve in this way is shown in Fig. 4(b), which is plotted by the same parameters with Fig. 3. The proposed method is a bit similar to GO-CFAR [37], which takes the maximum of the background pixels as the power of clutter to control PFA in the edge of clutter, in some ways. Here, our solution use the maximum of the joint pixels as the power of moving targets to improve PD. So, we call our solution GO-DPCA here

Besides, to improve PD so that decreasing detection missings further, we can use a lower detection threshold when performing CFAR here. The decrease of threshold can be implemented by the relationships between PD, PFA and the threshold, which are derived as below. Let $I_{c,m}$, $I_{n,m}$, and $I_{t,m}$ denote the component of clutter, noise and moving targets obtained from the mth channel in the postsuppression domain, respectively. Assume that $I_{c,m}$ and $I_{n,m}$ follow the zero mean complex Gaussian distribution with variance σ_c^2 and σ_n^2, respectively [33] while the moving target is supposed to follow the fluctuating model of Swerling case I [34]. Then the following two hypothesis testings are given as (12) where H_0 denotes the pixels which do not contain moving targets and H_1 denotes the pixels which contain moving targets. k is the sequence number of the pixels used for multilook in a K-look SAR image

$$\begin{cases} H_0 : \rho = \sqrt{\frac{1}{K} \sum_{k=1}^{K} |I_{c,m}(k) + I_{n,m}(k)|^2} \\ H_1 : \rho = \sqrt{\frac{1}{K} \sum_{k=1}^{K} |I_{t,m}(k) + I_{c,m}(k) + I_{n,m}(k)|^2} \end{cases}. \quad (12)$$
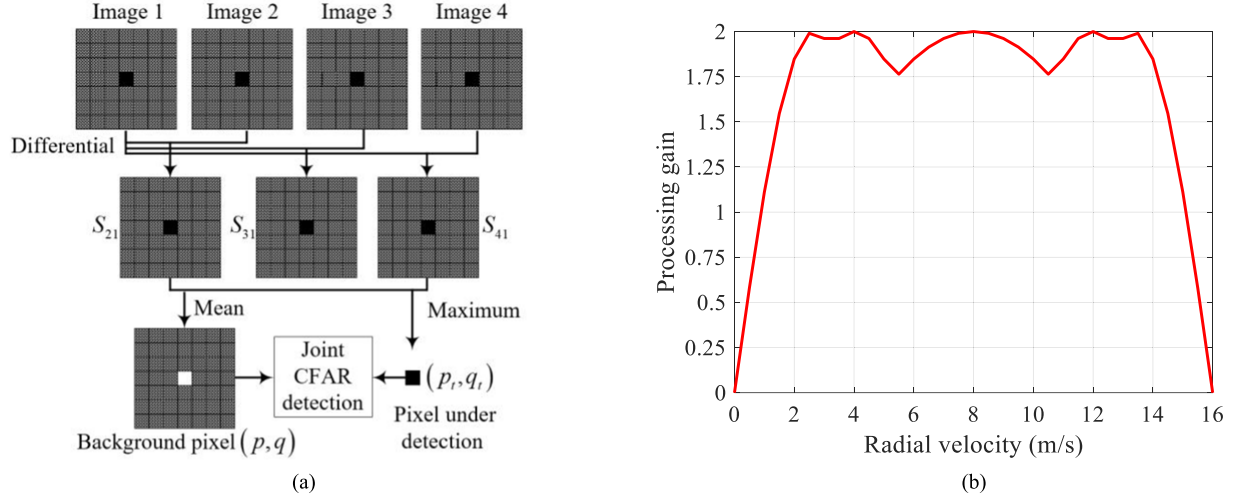
Fig. 4. Description of the GO-DPCA. (a) Flow chart of the GO-DPCA. (b) Theoretical gain of moving targets obtained from GO-DPCA.

The statistics of these two hypothesis testings follow the square root of gamma distribution with different parameters [35], [36]. The probability density functions (PDF) are formulated as

$$\begin{cases} P\left(\rho|H_0\right) = \frac{2}{\Gamma(\alpha)} \cdot \beta_1^\alpha \cdot \rho^{2\alpha-1} \cdot \exp\left(-\beta_1 \cdot \rho^2\right) \\ P\left(\rho|H_1\right) = \frac{2}{\Gamma(\alpha)} \cdot \beta_2^\alpha \cdot \rho^{2\alpha-1} \cdot \exp\left(-\beta_2 \cdot \rho^2\right) \end{cases} \quad (13)$$

where $\Gamma(\cdot)$ denotes the gamma function. The value of shape parameter α equals K. The scale parameters β_1 and β_2 can be expressed as

$$\beta_1 = \alpha/\sigma_{cn}^2 \quad (14)$$

$$\beta_2 = \alpha/\left(\delta \cdot \sigma_s^2 + \sigma_{cn}^2\right) \quad (15)$$

where σ_{cn}^2 is the power of residual clutter plus noise in the postsuppression domain. σ_s^2 denotes the power of moving targets in the original image domain. δ denotes the processing gain of moving targets generally. Then, the PFA and the PD can be derived as (16) and (17), respectively, shown at the bottom of this page. Assume that the channel errors can be well corrected and σ_{cn}^2 of different baseline length and methods are basically same. Then we can see that the difference of the processing gain

will influence PD by changing the value of the scale parameters. Thus, (16) and (17), can also show the advantage of GO-DPCA on improving PD.

C. Step II- Local Adaptive Process in Original Image Domain for Clutter Suppression and Radial Velocity Estimation Simultaneously.

After step I, the position of each moving target is known now. So only the local data of the detected targets needed to be processed. Since the moving targets usually distribute sparsely in the scene, most pixels which do not contain the moving target can be ignored. Then, a lot of computational burden can be avoided. In step II, we directly extract the useful data in the original image domain for clutter suppression and radial velocity estimation by local STAP simultaneously. In practice, the inevitable registration errors and defocusing of moving targets will degrade the accuracy of covariance matrix estimating. To avoid the occurance of the performance degrading. There are two types of joint pixel model in the current papers [30], [38]–[40]. First one, we can call it ' suppressing one point by multiple points '[30], [38]. It means that using the joint pixels from channel 2 to channel M to suppress the target pixel of the first channel.

$$P_{fa} = \int_\eta^\infty P\left(\rho|H_0\right) d\rho$$

$$= 1 - \frac{2\beta_1^\alpha}{\Gamma(\alpha)} \left[\left(\frac{1}{2\beta_1}\right)^\alpha \prod_{h=1}^{\alpha-1} (2\alpha - 2h) - \frac{\eta^{2\alpha-2}}{2\beta_1} \exp\left(-\beta_1\eta^2\right) - \sum_{j=2}^\alpha \left(\frac{1}{2\beta_1}\right)^j \prod_{h=1}^{j-1} (2\alpha - 2h)\, \eta^{2\alpha-2j} \exp\left(-\beta_1\eta^2\right) \right] \quad (16)$$

$$P_d = \int_\eta^\infty P\left(\rho|H_1\right) d\rho$$

$$= 1 - \frac{2\beta_2^\alpha}{\Gamma(\alpha)} \left[\left(\frac{1}{2\beta_2}\right)^\alpha \prod_{h=1}^{\alpha-1} (2\alpha - 2h) - \frac{\eta^{2\alpha-2}}{2\beta_2} \exp\left(-\beta_2\eta^2\right) - \sum_{j=2}^\alpha \left(\frac{1}{2\beta_2}\right)^j \prod_{h=1}^{j-1} (2\alpha - 2h)\, \eta^{2\alpha-2j} \exp\left(-\beta_2\eta^2\right) \right] \quad (17)$$
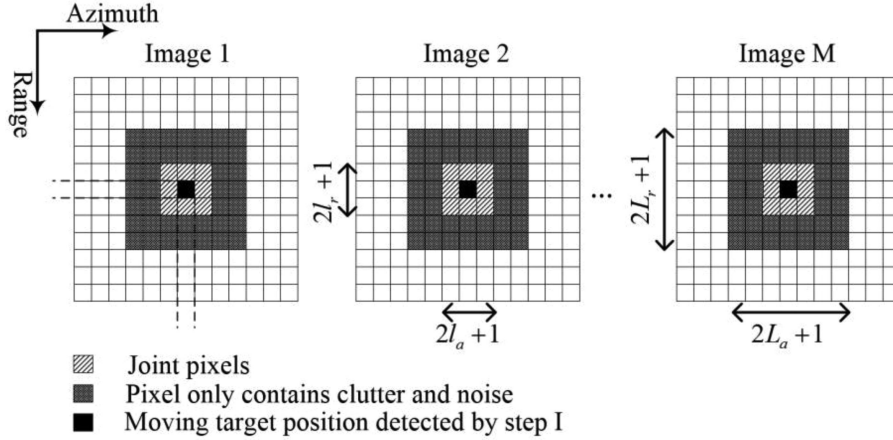
Fig. 5.   Extracted model of data in step II.

Second one, we can call it ' suppressing multiple points by multiple points '[39], [40]. It means that using the joint pixels from channel 1 to channel M to suppress the target pixels of all M channels. Here we select the second model. As shown in Fig. 5, the extracted local data can be expressed as

$$Z_1 = [i\,(p_t - L_r, q_t - L_a)\,,\ldots, i\,(p_t, q_t)\,,\ldots,$$
$$i\,(p_t + L_r, q_t + L_a)]$$
$$\in C^{M \times L} \tag{18}$$
$$Z_2 = [i\,(p_t - l_r, q_t - l_a)\,,\ldots, i\,(p_t, q_t)\,,\ldots,$$
$$i\,(p_t + l_r, q_t + l_a)]$$
$$\in C^{M \times l} \tag{19}$$

where the vector i can be represented as (20)

$$i\,(p_t, q_t) = [S_1\,(p_t, q_t)\,, S_2\,(p_t, q_t)\,,\ldots, S_M\,(p_t, q_t)]^T.$$
$$\in C^{M \times 1} \tag{20}$$

The black pixel means the position of the moving target detected by Step I with coordinate (p_t, q_t). The oblique stripe pixels mean the joint pixels of moving targets. These two kind of pixels contain the signal of moving target plus clutter and noise, which can be formulated as (20). The shadow pixels outside the joint pixels denote the pixels only contain clutter and noise.

Then the covariance matrix of the signal that only contains clutter and noise can be estimated from

$$\hat{r} = \frac{1}{L - l} Z_3 Z_3^H \tag{21}$$

where Z_3 denotes the supplementary set of Z_2 with the full set Z_1. l and L are expressed as

$$\begin{cases} l = (2l_r + 1) \cdot (2l_a + 1) \\ L = (2L_r + 1) \cdot (2L_a + 1) \end{cases} . \tag{22}$$

Then, linear constraint minimum variance algorithm is applied for clutter suppression and radial velocity estimation simultaneously, which can be described as

$$\begin{cases} \min \omega_{\mathrm{opt}}^H \hat{r} \omega_{\mathrm{opt}} \\ \text{s.t. } \omega_{\mathrm{opt}}^H G = Q^H \end{cases} \tag{23}$$

where $G = [a_t, a_c] \in C^{M \times 2}$ and $Q = [1, 0]^T$. And the optimum weight vector can be derivated as

$$\omega_{\mathrm{opt}} = \hat{r}^{-1} G (G^H \hat{r}^{-1} G)^{-1} Q. \tag{24}$$

Then, radial velocity and azimuth offset can be estimated as

$$\hat{v}_r = \underset{v_r}{\arg\max} \overline{\left| \omega_{\mathrm{opt}}^H Z_2\,(v_r) \right|^2} \Big/ \overline{\left| \omega_{\mathrm{opt}}^H Z_3\,(v_r) \right|^2} \tag{25}$$

$$\Delta f_a = \frac{2\widehat{v}_r}{\lambda} \tag{26}$$

where $\bar{\,\cdot\,}$ denotes the mean value of the matrix.

The flow chart of the proposed two-step scheme is given in Fig. 6. The output of local STAP is used for moving targets detection again to eliminate the extra false alarms caused by step I.

IV.   EXPERIMENTAL RESULTS AND DISCUSSION

A. Simulated Data Results

As shown in Fig. 7, we use an acquired complex SAR image with main parameters given in Table I. Then, the image is transformed back to the 2-D signal domain as the signal of clutter and noise. We use same the parameters to simulate the signal of 33 moving targets whose radial velocity are ranged from 0 to 16m/s with the interval of 0.5 m/s in an individual period of radial velocity. Then these two types of signal are mixed as the initial simulated SAR-GMTI data.

First, we use conventional DPCA and the proposed GO-DPCA to suppress the clutter, respectively, and extract the residual amplitude of the pixels where each simulated moving target locate in. The results are shown in Fig. 8. We can see that the clutter is well suppressed. Thus, the residual amplitude is mainly decided by moving targets. The experimental curves
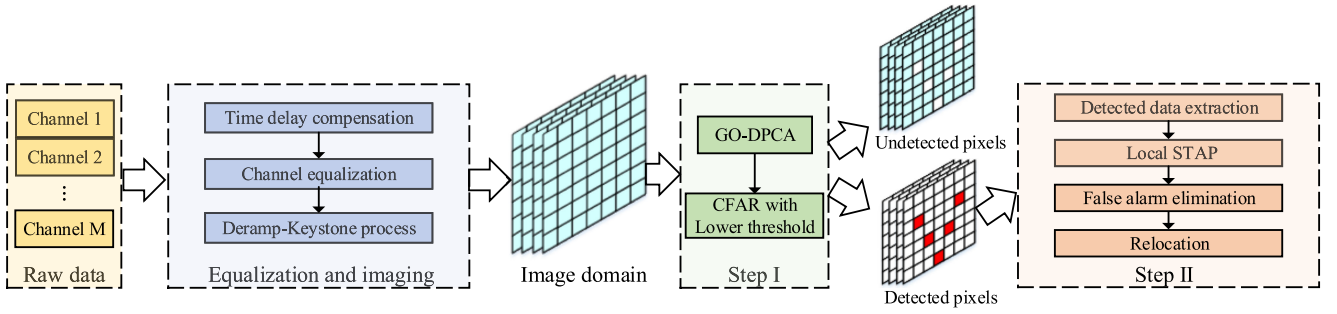
Fig. 6. Flow chart of the proposed two-step scheme (red pixels denote the position of the moving targets detected in step I).
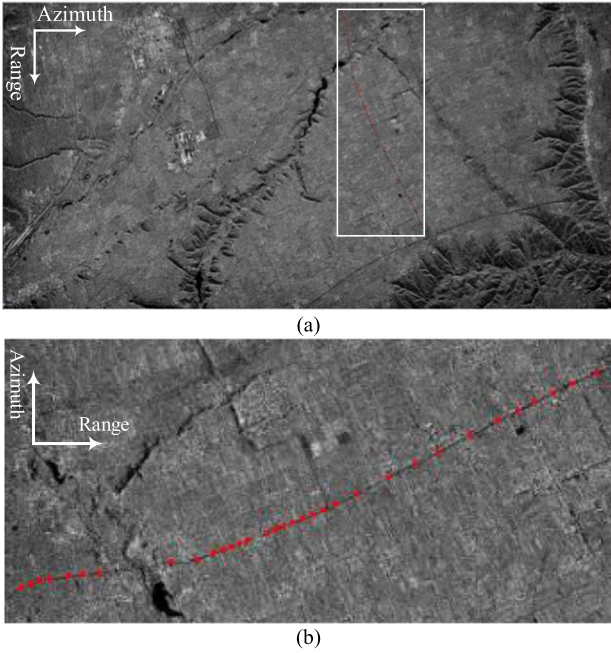

Fig. 7. Acquired SAR image used for simulation (red points are the positions of 33 moving targets we simulated). (a) Whole image. (b) Enlarged image of the road which are plotted by the white box in (a).

TABLE II
MAIN PARAMETERS OF AQUIRED DATA

Parameter	Value
Bandwidth	18MHz
Slant range	40km
Array spacing	0.6m
Channel number	3
Platform velocity	120m/s
Carrier frequency	9.6GHz
Pulse repetition frequency	800Hz

have the same results with the theoretical gain curves in the Figs. 3 and 4(b). Of course there is still some residual clutter and noise, which makes the experimental curves not as symmetrical as the theoretical ones.

Then we plot the receiver operation characteristic (ROC) curve of the proposed GO-DPCA. For comparison, we select ID-ATI on behalf of the conventional nonadaptive method, which utilizes the images obtained from adjacent channels to suppress clutter. As shown in Fig. 9(a) and (b), the x-axis, y-axis, and z-axis denote the PFA, radial velocity and PD, respectively. It' worth mentioning that only the images from adjacent channels can be used for image differential and further ATI process in case of three or four channels because of the Specific phase relationship [41]. Therefore, we plot the curve of ID-ATI by the calculation of Δ_2 here. We can see that the notch of GO-DPCA is narrower than ID-ATI, which means better detection performance. To validate this theoretical results, 150 Monte Carlo experiments are made here in the case of

$\text{PFA} = 10^{-6}$ with the result shown in Fig. 9(c). It illustrates that the experimental result is basically coincident with the theoretical one. The detection performance of GO-DPCA is better than ID-ATI. In terms of the goal in step I, GO-DPCA is a better choice.

In practical application, the standard which is utilized to measure whether a ground moving target can be detected is usually set as $\text{PD} \geq 0.9$ when $\text{PFA} = 10^{-6}$. Thus, we select the moving targets whose PD are higher than 0.9 obtained from each method for 150 Monte Carlo experiments again to estimate their radial velocity. Then, we use the mean value of the estimation results to relocate each moving target. The final relocation results are given in Fig. 10. The red point means the relocated position of each simulated moving target. The yellow arrow directs to the relocated position of the simulated moving target from its original position. We can see that the GO-DPCA detect more moving targets than ID-ATI and has better relocation accuracy.

B. Acquired Data Results

In order to verify the correctness and effectiveness of the proposed two-step scheme, a measured data obtained from an airborne SAR-GMTI system with main parameters given in Table II is processed. As shown in Fig. 13(a), the experimental site is near an airport in Yanniang. There are three main roads in range which are marked by red arrows. Some noncooperative moving targets are travelling on it.

First, time-delay compensation and channel equalization are performed in 2-D signal domain. After that, we can get the SAR images of each channel in range-Doppler domain by DKP. Then the complex images of channels 2 and 3 are utilized to achieve
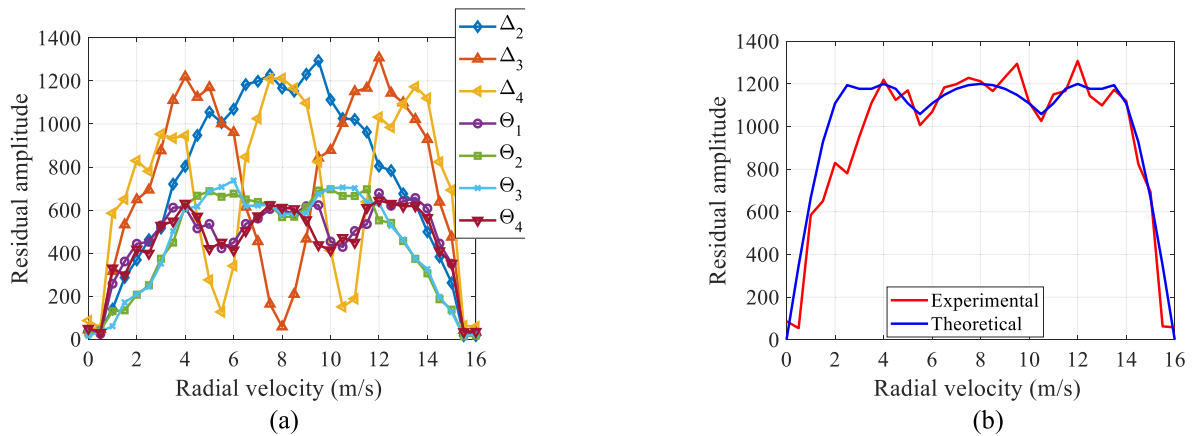
Fig. 8. Residual amplitude of the simulated moving targets. (a) Conventional DPCA. (b) Greatest of- displaced phase center antenna.
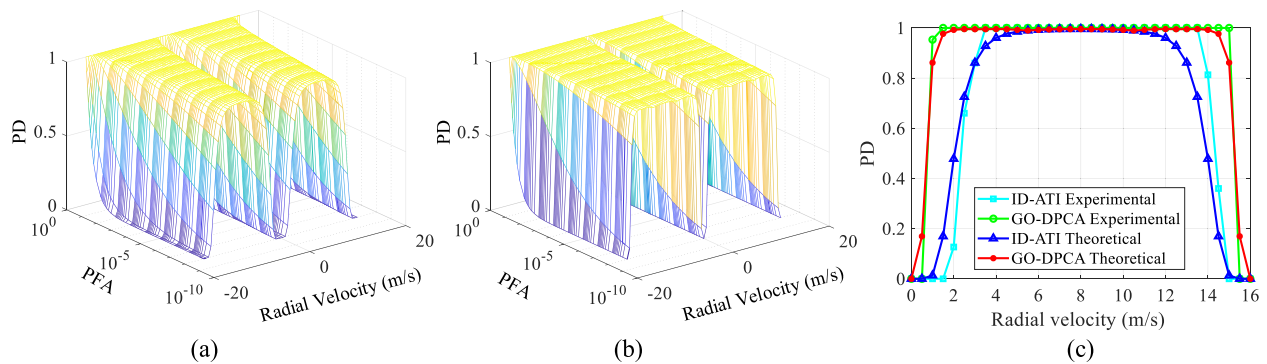

Fig. 9 Analysis on detection performance. (a) ROC curve of ID-ATI. (b) ROC curve of GO-DPCA. (c) Results of 150 Monte Carlo experiments.
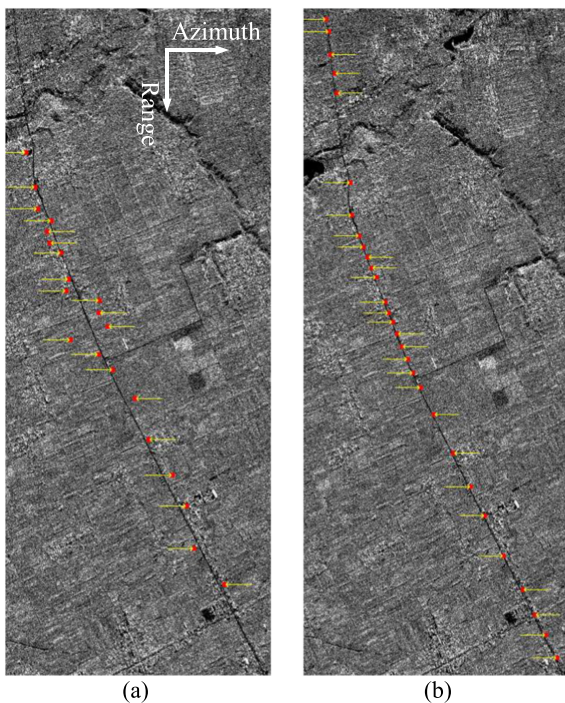

Fig. 10. Relocation results of moving targets. (a) ID-ATI. (b) Greatest of-displaced phase center antenna.

image differential with that of channel 1 for clutter suppression, respectively. Fig. 11(a) shows the SAR images of channel 1 and the clutter suppression results are shown in Fig. 11(b) and (c), respectively, with the same quantification. We can see that the clutter is well suppressed and the residual signal of moving targets can be seen now. We have selected the pixels which do not contain moving targets according to the results of CFAR from the real data and counted their distribution to validate (13) and (14). The value of α is 4 here. The mean power of the residual clutter and noise is 4.6865×10^8, which means that $\sigma_{cn}^2 = 4.6865 \times 10^8$ in (14). Then, we have calculated and plotted the theoretical curve by (13) and (14). The results are given in the Fig. 12. It illustrates that the theoretical curve can be basically consistent with the curve of real data. Then, the detection results are shown in Fig. 13(d) where green points denote the positions of detected moving targets. These targets are displaced away the roads because of the radial velocity. Then, we extract the signal of detected moving targets from original image domain for local STAP to suppress clutter and estimate radial velocity simultaneously. The estimated velocity are used for relocation with results shown in Fig. 13(d) as well. The red points denote the relocation positions and they are connected with the displaced positions by yellow arrows. We can see that the moving targets are setting on the roads again after relocation.
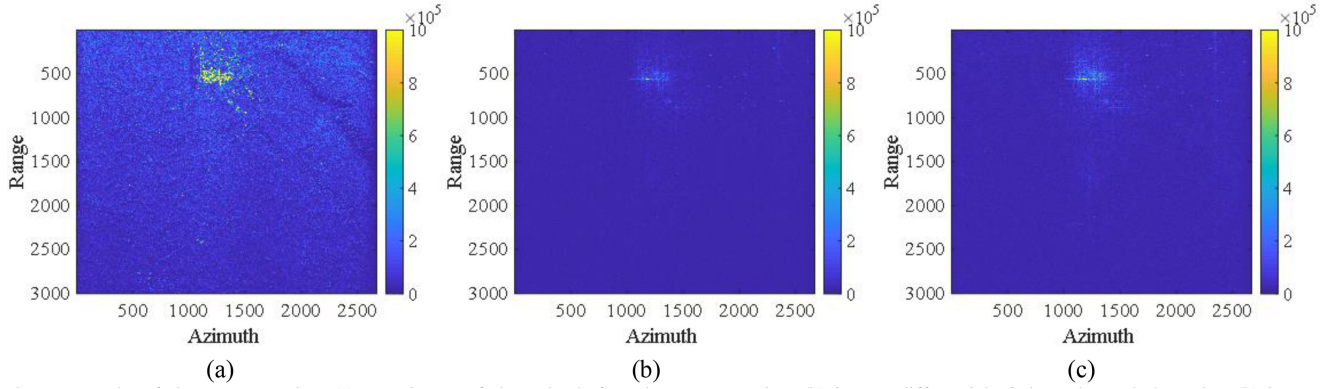
Fig. 11. Results of clutter suppression. (a) SAR image of channel 1 before clutter suppression. (b) Images differential of channels 1 and 2. (b) Images differential of channel 1 and channel 3.
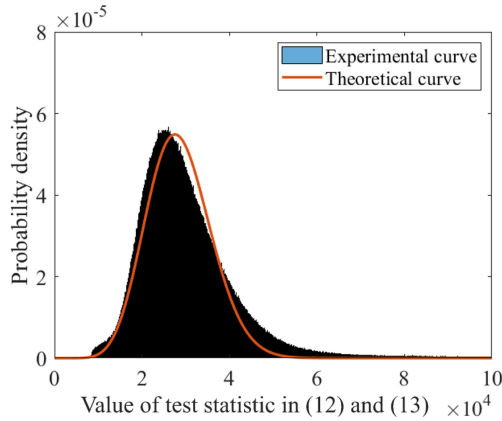

Fig. 12. Clutter distribution in the postsuppression domain.

We use ID-ATI and STAP for comparison here with results shown in Fig. 13(b) and (c), respectively. We can see that ID-ATI has lost 14 moving targets which are marked by the white circles compared to STAP while GO-DPCA has lost only five targets. And the relocation results of some moving targets obtained from ID-ATI is worse than that from GO-DPCA, which is caused by the signal loss of moving targets in the postsuppression domain. The result can validate that GO-DPCA has better detection performance and can realize the goal of step I better than conventional DPCA.

Then, we select two moving targets which are marked in Fig. 13(c) for further analysis. Target A has been detected only by STAP while target B has been detected by STAP and GO-DPCA. Figs. 14 and 15 show the local images of targets A and B in the postsuppression domain, respectively. Fig. 16 shows the improvement factor (IF) curves of the experimental SAR-GMTI system when assuming the initial SCNR is -40 dB. The radial velocities of target A and B estimated by the proposed method are -6.15 and 5.9 m/s, respectively. We can see that radial velocity of the target A is more close to the blind velocity where the IF curves of ID-ATI and GO-DPCA decrease rapidly. Thus,

the SCNR of target A obtained from ID-ATI and GO-DPCA is not enough for detection. For target B, its SCNR obtained from GO-DPCA is high enough for detecion while that of ID-ATI is still relative low. Thus, target B hasn't detected by ID-ATI while GO-DPCA has detected it. STAP has narrower notch and better performance. Thus, it has detected both of target A and target B.

C. Computational Complexity Analysis

In this part, we will analyze the computational complexity of the proposed joint two-step scheme compared to that of the conventional nonadaptive and adaptive methods to show the efficiency of the proposed method. Here we select ID-ATI and STAP to represent the nonadaptive and adaptive methods, respectively. We have calculated the number of floating-point operation (FLOP) of three methods after imaging process according to [42], [43]. A complex multiplication contains six real FLOPS and a complex summation contains two real FLOPS. The results are given in Table III. N_r and N_a denote the number of pixels in the SAR image, respectively. N_v is the number of radial velocity when searching the maximum of test statistics in each pixel. Assume that there are N_t pixels which contain moving targets. It's worth mentioning that we use $1.5N_t$ to calculate the computational complexity of the proposed method considering the extra false alarms after step I. Then we plot the computational complexity curves of three methods according to Table III with $N_r = 4096$, $N_a = 2048$, $N_v = 60$, $M = 3$, $L = 25$, and $l = 9$. Fig. 17 illustrates that the computational complexity of the proposed joint two-step scheme will increase as the N_t increase. Considering moving targets usually distribute sparsely in the scene, the number of moving targets in a SAR image with the normal size is in the magnitude order of 10^1 or 10^2, which is marked by the red circle in Fig. 17. In this region of N_t, the computational complexity of the proposed joint two-step scheme is far less than that of STAP and a bit higher than that of ID-ATI.
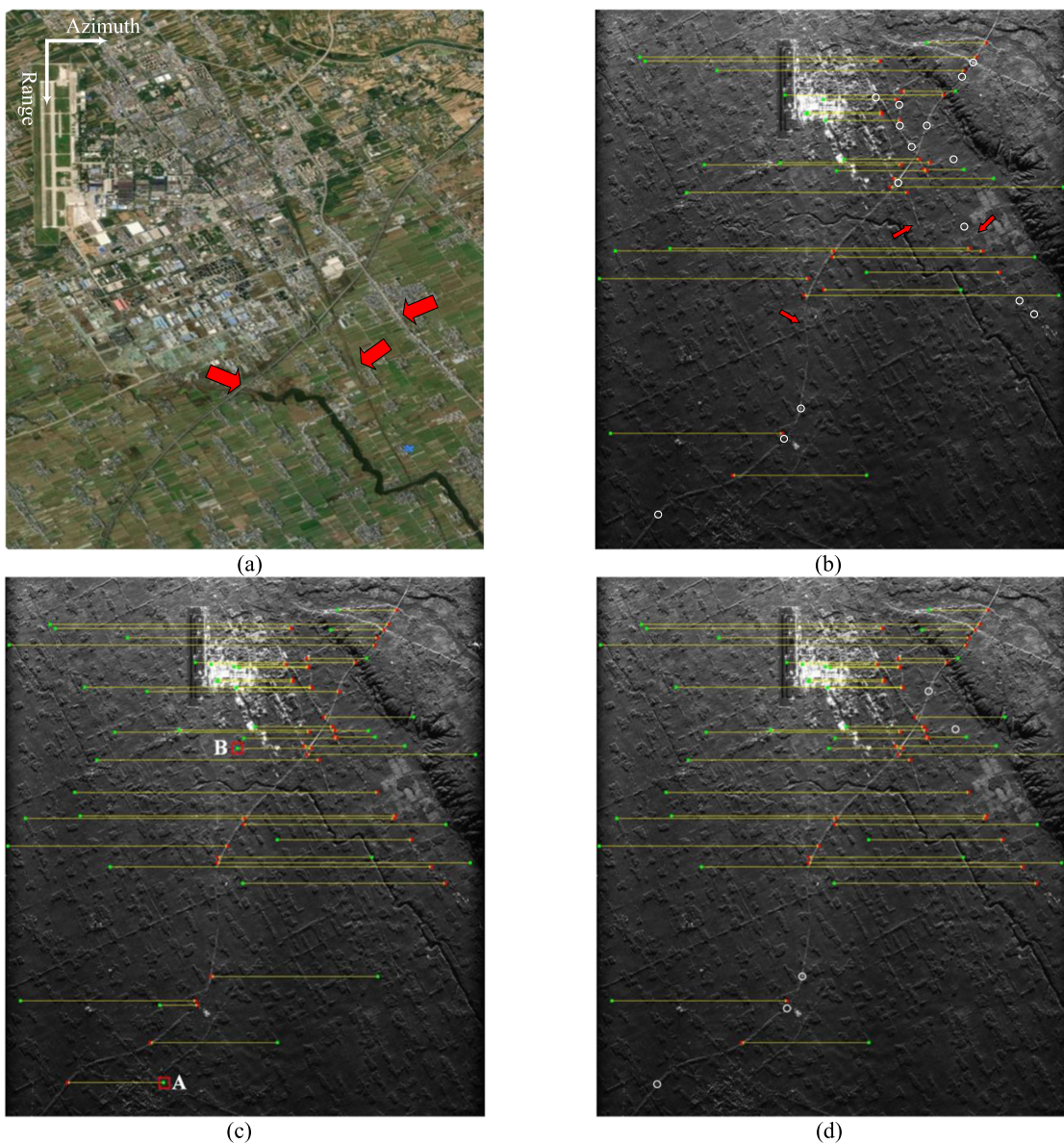
Fig. 13. Results of moving targets detection and relocation. (a) Optical image of the experimental scene. (b) ID-ATI (three main roads are marked by red arrows). (c) Space-time adaptive processing. (d) Proposed (the white circles denote the missing moving targets of each method. Green and red points denote the positions before and after relocation, respectively).
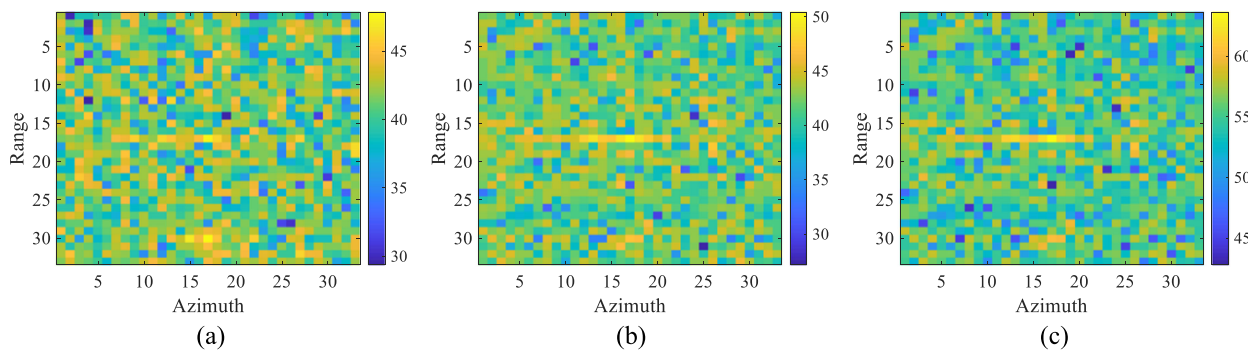

Fig. 14. Local image of target A in postsuppression domain. (a) Images differential -along-track interferometry. (b) Greatest of-displaced phase center antenna. (d) Space-time adaptive processing(the unit of colorbar is dB).
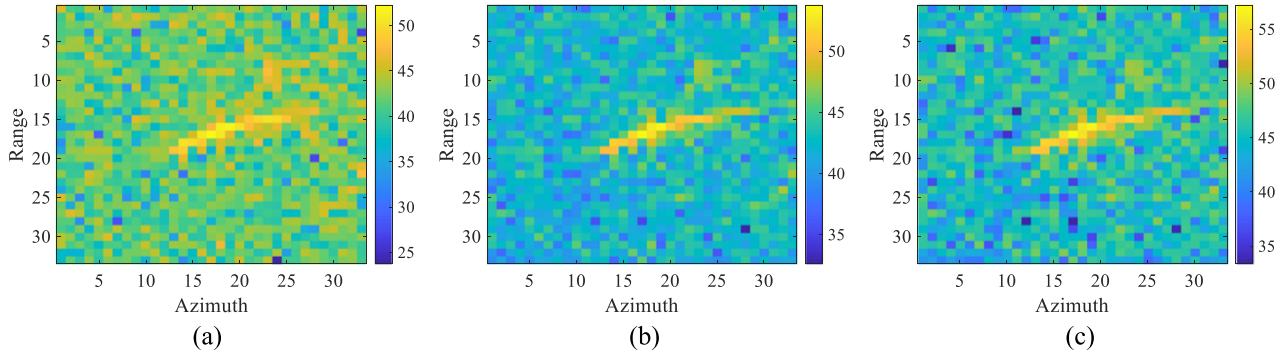
Fig. 15.   Local image of target B in postsuppression domain. (a) Images differential-along-track interferometry. (b) Greatest of -displaced phase center antenna. (d) Space-time adaptive processing (the unit of colorbar is dB).

TABLE III
COMPUTATIONAL COMPLEXITY OF THREE METHODS

| Method	Concrete operation	Number of complex multiplications	Number of complex summations
ID-ATI	Image differential	0	$2N_r N_a$
	CFAR	$\dfrac{3N_r N_a \left(\log_2 N_a + \log_2 N_r \right)}{2}$	$3N_r N_a \left(\log_2 N_a + \log_2 N_r \right) + N_r N_a$
	ATI	N_t	0
STAP	Calculate covariance matrix	$N_r N_a \cdot \left(2M^2 \left(L - l \right) \right)$	0
	Calculate inverse of covariance matrix	$N_r N_a \cdot \left(M^3 + M^2 + M \right)$	0
	Calculate optimal weight and suppression	$N_r N_a N_v \cdot \left(8M^2 + 13M + 2ML + 10 - l \right)$	0
Proposed	Image differential	0	$\left(M - 1 \right) \cdot N_r N_a$
	CFAR	$\dfrac{3N_r N_a \left(\log_2 N_a + \log_2 N_r \right)}{2}$	$3N_r N_a \left(\log_2 N_a + \log_2 N_r \right) + N_r N_a$
	Calculate covariance matrix	$1.5N_t \cdot \left(2M^2 \left(L - l \right) \right)$	0
	Calculate inverse of covariance matrix	$1.5N_t \cdot \left(M^3 + M^2 + M \right)$	0
	Calculate optimal weight and suppression	$1.5N_t N_v \cdot \left(8M^2 + 13M + 2ML + 10 - l \right)$	0
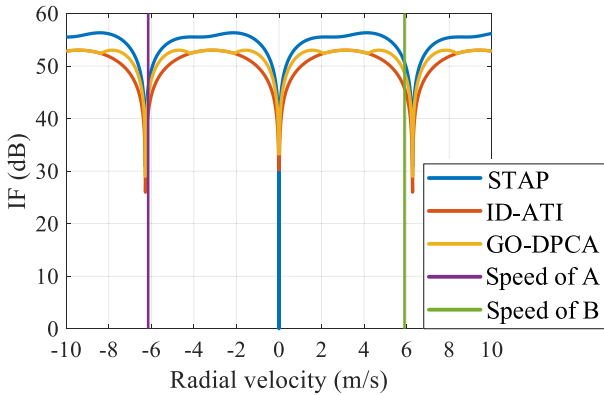
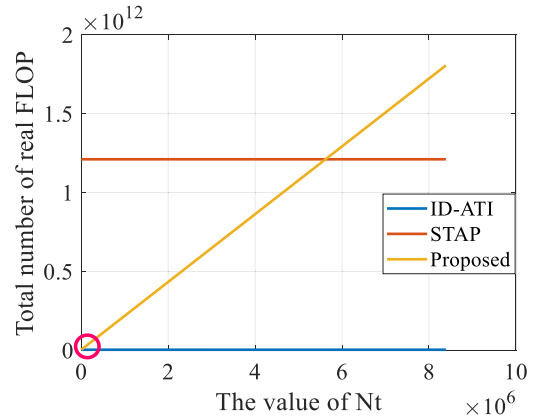Fig. 16.   IF curves of the experimental SAR-GMTI system.

Fig. 17.   Comparison of the computational complexity.

V. CONCLUSION

In this article, a novel two-step scheme based on GO-DPCA and local STAP in image domain is proposed for multichannel SAR-GMTI systems.

Since the adaptive methods suppress clutter and estimate radial velocity in one step simultaneously while the position and radial velocity of each moving target are unknown at first. The adaptive methods need to calculate the convariance matrix and search the maximum of test statistics pixel by pixel over a large range of radial velocity, which will bring heavy computational burden. As moving targets usually distribute sparsely in the scene, which means that the search of most pixels will be in vain. The main idea of this article is to separate the achievement of clutter suppression and radial velocity estimation into two parts. Step I is used for clutter suppression and moving targets detection to find their positions by the nonadaptive method. Then, in step II, only the local data of the moving targets detected in step I need to be processed. In this way, a big part of computational burden can be avoided.

Besides, the key point of step I is trying to avoid detection missing of moving targets compared to the adaptive methods. So conventional nonadaptive methods, which will cause the signal loss of moving targets in postsuppression domain, need to be improved. After deriving the processing gain of moving targets obtained from conventional DPCA, we find that the gain will vary as the radial velocity and baseline length change. Thus, we propose GO-DPCA here, which can make the moving targets with different radial velocity all get their highest processsing gain.

Finally, the experiments of both simulated and acquired data are performed. The results show that the proposed method can basically get close results compared to STAP while a big part of computational burden can be avoided, which proves that the proposed method can be useful in practical application.

APPENDIX I
DETAILED DERIVATIONS OF (4)

After time delay compensation and channel equalization, the echo of the mth channel has got a time shift in azimuth with d_m/v_a. Therefore, the equivalent slant range can be expressed as

$$
R_m \left(t_a - \frac{d_m}{v_a} \right) \approx \frac{(v_a - v_x)^2}{2R_B} t_a^2
$$
$$
+ \left(v_r - \frac{(v_a - v_x) X_n}{R_B} - \frac{v_x}{v_a} \frac{(v_a - v_x) d_m}{R_B} \right) t_a
$$
$$
+ R_B + \frac{X_n^2}{2R_B} - v_r \frac{d_m}{v_a} - \frac{v_x}{v_a} \frac{X_n d_m}{R_B} + \frac{v_x}{v_a} \frac{d_m^2}{R_B}. \quad (A1)
$$

The azimuth velocity of the moving target v_x is always far smaller than the velocity of the radar platform v_a. What's more, the interval of each channel d_m is far shorter than the slant range R_B as well. Therefore, we can assume $v_a \gg v_x$ and $R_B \gg d_m$. Then we can get $\frac{v_x}{v_a} \frac{(v_a - v_x) d_m}{R_B} \approx 0$, $\frac{v_x}{v_a} \frac{X_n d_m}{R_B} \approx 0$ and $\frac{v_x}{v_a} \frac{d_m^2}{R_B} \approx$

0. Therefore, the equivalent slant range can be rewritten as

$$
R_m \left(t_a - \frac{d_m}{v_a} \right) \approx \frac{(v_a - v_x)^2}{2R_B} t_a^2
$$
$$
+ \left(v_r - \frac{(v_a - v_x) X_n}{R_B} \right) t_a + R_B + \frac{X_n^2}{2R_B} - v_r \frac{d_m}{v_a}. \quad (A2)
$$

Finally, we can get the form of (4)

$$
R_{res} = R_B + \frac{X_n^2}{2R_B} - v_r \frac{d_m}{R_B}. \quad (A3)
$$

APPENDIX II
DETAILED DERIVATIONS OF (16) AND (17)

According to the PDF given in (13) and the definition of PFA, the PFA can be calculated by the integral shown as

$$
P_{fa} = \int_\eta^\infty \frac{2\beta_1^\alpha}{\Gamma(\alpha)} \cdot \rho^{2\alpha-1} \cdot \exp\left(-\beta_1 \rho^2\right) d\rho. \quad (B1)
$$

The meanings of each notation have been given below the manuscript. First, the primitive function of the indefinite integral is derived. Using integral by substitution, let $\sigma = -\beta_1 \rho^2$, then we can get

$$
d\sigma = -2\beta_1 \rho \cdot d\rho. \quad (B2)
$$

Let $v = \exp(-\beta_1 \rho^2) = \exp(\sigma)$, then we can get

$$
dv = \exp(\sigma) d\sigma = -2\beta_1 \rho \cdot \exp\left(-\beta_1 \rho^2\right) d\rho. \quad (B3)
$$

Let $u = -\frac{1}{2\beta_1} \rho^{2\alpha-2}$, then the indefinite integral can be rewritten as

$$
\int \rho^{2\alpha-1} \cdot \exp\left(-\beta_1 \rho^2\right) d\rho = \int u \cdot dv. \quad (B4)
$$

According to (4), we get the form of the integral by parts. Then for the first time integral, we can get the results expressed as

$$
\int \rho^{2\alpha-1} \cdot \exp\left(-\beta_1 \rho^2\right) d\rho = -\frac{1}{2\beta_1} \rho^{2\alpha-2} \exp\left(-\beta_1 \rho^2\right)
$$
$$
+ \frac{2\alpha-2}{2\beta_1} \int \rho^{2\alpha-3} \exp\left(-\beta_1 \rho^2\right) d\rho. \quad (B5)
$$

The last term of (5) can be calculated by the same way. Therefore, the second time integral can be formulated as

$$
\frac{2\alpha-2}{2\beta_1} \int \rho^{2\alpha-3} \cdot \exp\left(-\beta_1 \rho^2\right) d\rho
$$
$$
= -\left(\frac{1}{2\beta_1} \right)^2 (2\alpha-2) \rho^{2\alpha-4} \exp\left(-\beta_1 \rho^2\right)
$$
$$
+ \left(\frac{1}{2\beta_1} \right)^2 (2\alpha-2)(2\alpha-4) \int \rho^{2\alpha-5} \exp\left(-\beta_1 \rho^2\right) d\rho. \quad (B6)
$$

From (4) and (5), we can find the regularity of the integral results. The results of the jth time integral can be expressed as

$$
-\left(\frac{1}{2\beta_1} \right)^j (2\alpha-2)(2\alpha-4) \cdots (2\alpha-2j+2) \rho^{2\alpha-2j}
$$

$$\times \exp\left(-\beta_1 \rho^2\right) + \left(\frac{1}{2\alpha}\right)^2 (2\alpha - 2)(2\alpha - 4)\cdots(2\alpha - 2j)$$

$$\times \int \rho^{2\alpha - 2j - 1} \exp\left(-\beta_1 \rho^2\right) d\rho. \tag{B7}$$

When $j = \alpha$, the last term of (B7) equals to 0 and we can stop the integral. Therefore, according to (B5)–(B7), we can get the primitive function of the integral in (B1) expressed as

$$F(\rho) = \frac{2\beta_1^\alpha}{\Gamma(\alpha)} \cdot \left(-\frac{1}{2\beta_1}\rho^{2\alpha - 2}\exp\left(-\beta_1\rho^2\right) + \sum_{j=2}^{\alpha} -\left(\frac{1}{2\beta_1}\right)^j \right.$$

$$\left. \times \prod_{h=1}^{j-1}(2\alpha - 2h)\rho^{2a - 2j}\exp\left(-\beta_1\rho^2\right) \right). \tag{B8}$$

Note that $\rho \geq 0$, then PFA can be calculated as

$$P_{fa} = 1 - (F(\eta) - F(0))$$

$$= 1 - \frac{2\beta_1^\alpha}{\Gamma(\alpha)}\left(\left(\frac{1}{2\beta_1}\right)^\alpha \prod_{h=1}^{\alpha-1}(2\alpha - 2h) - \frac{\eta^{2\alpha - 2}}{2\beta_1}\exp\left(-\beta_1\eta^2\right) \right.$$

$$\left. - \sum_{j=2}^{\alpha}\left(\frac{1}{2\beta_1}\right)^j \prod_{h=1}^{j-1}(2\alpha - 2h)\eta^{2\alpha - 2j}\exp\left(-\beta_1\eta^2\right) \right). \tag{B9}$$

PD gets different scale parameter with PFA. Therefore, we can derive PD by the same way when replacing β_1 by β_2. Then, the result of PD can be expressed as

$$P_d = 1 - \frac{2\beta_2^\alpha}{\Gamma(\alpha)}\left(\left(\frac{1}{2\beta_2}\right)^\alpha \prod_{h=1}^{\alpha-1}(2\alpha - 2h) - \frac{\eta^{2\alpha - 2}}{2\beta_2} \right.$$

$$\times \exp\left(-\beta_2\eta^2\right) - \sum_{j=2}^{\alpha}\left(\frac{1}{2\beta_2}\right)^j \prod_{h=1}^{j-1}(2\alpha - 2h)\eta^{2\alpha - 2j}$$

$$\left. \times \exp\left(-\beta_2\eta^2\right) \right). \tag{B10}$$

REFERENCES

[1] J. Chen, M. Xing, X.-G. Xia, J. Zhang, B. Liang, and D.-G. Yang, "SVD-based ambiguity function analysis for nonlinear trajectory SAR," *IEEE Trans. Geosci. Remote Sens.*, vol. 59, no. 4, pp. 3072–3087, Apr. 2020.

[2] Z. Li *et al.*, "Focusing of maneuvering high-squint-mode SAR data based on equivalent range model and wavenumber-domain imaging algorithm," *IEEE J. Sel. Topics Appl. Earth Observ. Remote Sens.*, vol. 13, pp. 2419–2433, 2020.

[3] S. Li, S. Mei, S. Zhang, S. Wan, and T. Jia, "A novel compressive sensing-based multichannel HRWS SAR imaging technique for moving targets," *IEEE J. Sel. Topics Appl. Earth Observ. Remote Sens.*, vol. 14, pp. 690–703, 2021.

[4] F. Zhou, J. Yang, G. Sun, and J. Zhang, "A real-time imaging processing method based on modified RMA with sub-aperture images fusion for spaceborne spotlight SAR," in *Proc. IEEE Int. Geosci. Remote Sens. Symp.*, Sep. 2020, pp. 1905–1908.

[5] W. Li, Z. Xu, and D. Zhu, "The FPGA implementation of real-time spotlight SAR IMAGING," in *Proc. IEEE Int. Geosci. Remote Sens. Symp.*, Jul. 2018, pp. 6703–6706.

[6] J. Chen, J. Zhang, Y. Jin, H. Yu, B. Liang, and D. -G. Yang, "Real-time processing of spaceborne SAR data with nonlinear trajectory based on variable PRF," *IEEE Trans. Geosci. Remote Sens.*, to be published, doi: 10.1109/TGRS.2021.3067945.

[7] Y. Xiong, B. Liang, H. Yu, J. Chen, Y. Jin, and M. Xing, "Processing of bistatic SAR data with nonlinear trajectory using a controlled-SVD algorithm," *IEEE J. Sel. Topics Appl. Earth Observ. Remote Sens.*, vol. 14, pp. 5750–5759, 2021.

[8] H. Bi, G. Bi, B. Zhang, and W. Hong, "Real-time data processing in sparse SAR imaging," in *Proc. IEEE 11th Int. Conf. Adv. Infocomm Technol.*, 2019, pp. 228–231.

[9] M. V. Dragoševic and C. E. Livingstone, "Demonstration of ´RADARSAT-2 moving object detection experiment (MODEX) capabilities for maritime surveillance," in *Proc. IRS*, Sep. 2009, pp. 83–87.

[10] E. Makhoul, S. V. Baumgartner, M. Jäger, and A. Broquetas, "Multichannel SAR-GMTI in maritime scenarios with F-SAR and TerraSAR-X sensors," *IEEE J. Sel. Top. Appl. Earth Observ. Remote Sens.*, vol. 8, no. 11, pp. 5052–5067, Nov. 2015.

[11] D. Weihing, S. Suchandt, S. Hinz, H. Runge, and R. Bamler, "Traffic parameter estimation using TerraSAR-X data," *Int. Arch. Photogram. Remote Sens. Spatial Inf. Sci.*, vol. 61, pp. 153–156, 2008.

[12] R. Klemm, "Introduction to space–time adaptive processing," *Electron. Commun. Eng. J.*, vol. 11, no. 1, pp. 5–12, Feb. 1999.

[13] J. Ward, *Space–Time Adaptive Processing For Airborne Radar*. Lexington, MA, USA: MIT Lincoln Lab., Dec. 1994.

[14] K. Duan, H. Xu, H. Yuan, H. Xie, and Y. Wang, "Reduced-DOF three-dimensional STAP via subarray synthesis for nonsidelooking planar array airborne radar," *IEEE Trans. Aerosp. Elect. Syst.*, vol. 56, no. 4, pp. 3311–3325, Aug. 2020.

[15] J. H. G. Ender, "Space-time processing for multichannel synthetic aperture radar," *Electron. Commun. Eng. J.*, vol. 11, no. 1, pp. 29–38, Feb. 1999.

[16] D. Cerutti-Maori and I. Sikaneta, "Optimum GMTI processing for space-based SAR/GMTI systems—Theoretical derivation," in *Proc. Eur. Conf. Synthetic Aperture Radar*, Jun. 2010, pp. 1–4.

[17] D. Cerutti-Maori and I. Sikaneta, "Optimum GMTI processing for space-based SAR/GMTI systems—Simulation results," in *Proc. Eur. Conf. Synthetic Aperture Radar*, Jun. 2010, pp. 1–4.

[18] D. Cerutti-Maori, I. Sikaneta, and C. H. Gierull, "Optimum SAR/GMTI processing and its application to the radar satellite RADARSAT-2 for traffic monitoring," *IEEE Trans. Geosci. Remote Sens.*, vol. 50, no. 10, pp. 3868–3881, Oct. 2012.

[19] D. Cerutti-Maori and I. Sikaneta, "A generalization of DPCA processing for multichannel SAR/GMTI radars," *IEEE Trans. Geosci. Remote Sens.*, vol. 51, no. 1, pp. 560–572, Jan. 2013.

[20] G. Gao, X. Wang, and T. Lai, "Detection of moving ships based on a combination of magnitude and phase in along-track interferometric SAR—Part I: SIMP metric and its performance," *IEEE Trans. Geosci. Remote Sens.*, vol. 53, no. 7, pp. 3565–3581, Jul. 2015.

[21] C. H. Gierull, "Statistical analysis of multilook SAR interferograms for CFAR detection of ground moving targets," *IEEE Trans. Geosci. Remote Sens.*, vol. 42, no. 4, pp. 691–701, Apr. 2004.

[22] B. Li, G.C. Sun, M. Xing, Y. Hu, L. Guo, and Z. Bao, "Clutter suppression via subspace projection for spaceborne HRWS multichannel SAR system," *IEEE Geosci. Remote Sens. Lett.*, vol. 17, no. 9, pp. 1538–1542, Sep. 2020.

[23] H. S. C. Wang, "Mainlobe clutter cancellation by DPCA for space-based radars," in *Proc. IEEE Aerosp. Appl. Conf. Dig.*, 1991, pp. 1–128.

[24] S. Zhang, F. Zhou, G. Sun, X. Xia, M. Xing, and Z. Bao, "A new SAR–GMTI High-accuracy focusing and relocation method using instantaneous interferometry," *IEEE Trans. Geosci. Remote Sens.*, vol. 54, no. 9, pp. 5564–5577, Sep. 2016.

[25] H. Wang, H. Zhang, S. Dai, and Z. Sun, "Azimuth multichannel GMTI based on Ka-band DBF-SCORE SAR system," *IEEE Geosci. Remote Sens. Lett.*, vol. 15, no. 3, pp. 419–423, Mar. 2018.

[26] K. Suwa, K. Yamamoto, M. Tsuchida, S. Nakamura, T. Wakayama, and T. Hara, "Image-based target detection and radial velocity estimation methods for multichannel SAR-GMTI," *IEEE Trans. Geosci. Remote Sens.*, vol. 55, no. 3, pp. 1325–1338, Mar. 2017.

[27] L. Zhang, M.-D. Xing, C.-W. Qiu, and Z. Bao, "Adaptive two-step calibration for high-resolution and wide-swath SAR imaging," *IET Radar Sonar Navig.*, vol. 4, no. 4, pp. 548–559, Aug. 2010.

[28] H. Yan, R. Y. Wang, C. Gao, Y. B. Liu, M. Zheng, and Y. Deng, "Channel balancing algorithm in multichannel wide-area surveillance systems," *IET Radar Sonar Navig.*, vol. 8, no. 1, pp. 27–36, Jan. 2014.

[29] G. Sun, M. Xing, X. Xia, Y. Wu, and Z. Bao, "Robust ground moving-target imaging using deramp–keystone processing," *IEEE Trans. Geosci. Remote Sens.*, vol. 51, no. 2, pp. 966–982, Feb. 2013.

[30] Y. Shu, G. Liao, and Z. Yang, "Robust radial velocity estimation of moving targets based on adaptive data reconstruction and subspace projection algorithm," *IEEE Geosci. Remote Sens. Lett.*, vol. 11, no. 6, pp. 1101–1105, Jun. 2014.

[31] M. V. Dragosevic, W. Burwash, and S. Chiu, "Detection and estimation with RADARSAT-2 moving-object detection experiment modes," *IEEE Trans. Geosci. Remote Sens.*, vol. 50, no. 9, pp. 3527–3543, Sep. 2012.

[32] X. Zhang, *Matrix Analysis and Applications*, Beijing, China: Tsinghua Univ. Press, 2004.

[33] M. Preiss and N. J. S. Stacy, *Coherent Change Detection: Theoretical Description and Experimental Results*. Edinburgh, SA, Australia: Defence Sci. Technol. Org., 2006.

[34] P. Swerling, "Probability of detection for fluctuating targets," *IRE Trans. Inf. Theory.*, vol. 6, no. 2, pp. 269–308, Apr. 1960.

[35] D. Meyer and H. Mayer, *Radar Target Detection: Handbook of Theory and Practice*. New York, NY, USA: Academic, 1973.

[36] A. C. Frery, H. -J. Muller, C. C. F. Yanasse, and S. J. S. Sant'Anna, "A model for extremely heterogeneous clutter," *IEEE Trans. Geosci. Remote Sens.*, vol. 35, no. 3, pp. 648–659, May 1997.

[37] H. Rohling, "Radar CFAR thresholding in clutter and multiple target situations," *IEEE Trans. Aerosp. Elect. Syst.*, vol. AES-19, no. 4, pp. 608–621, Jul. 1983.

[38] X. He, G. Liao, J. Xu, and S. Zhu, "Robust radial velocity estimation based on joint-pixel normalized sample covariance matrix and shift vector for moving targets," *IEEE Geosci. Remote Sens. Lett.*, vol. 16, no. 2, pp. 221–225, Feb. 2019.

[39] Z. Li, Z. Bao, H. Li, and G. Liao, "Image autocoregistration and InSAR interferogram estimation using joint subspace projection," *IEEE Trans. Geosci. Remote Sens.*, vol. 44, no. 2, pp. 288–297, Feb. 2006.

[40] Z. Suo, Z. Li, and Z. Bao, "Multi-channel SAR-GMTI method robust to coregistration error of SAR images," *IEEE Trans. Aerosp. Electron. Syst.*, vol. 46, no. 4, pp. 2035–2043, Oct. 2010.

[41] X. Lv, J. Qian, M. Xing, and S. Zhang, "Results from an airborne Tri-channel SAR-GMTI experiment," in *Proc. Eur. Conf. Synthetic Aperture Radar*, 2008, pp. 1–4.

[42] R. Hunger, Floating point operations in matrix-vector calculus. Version 1.3, 2007. [Online]. Available: http://mediatum.ub.tum.de/doc/625604/625604.pdf

[43] Y. Ge, Z. -Z. Huang, Q. Liu, and Q. Lan, "Fast implementation of CA-CFAR algorithm based on FFT," in *Proc. IEEE 5th Adv. Inf. Technol., Electron. Automat. Control Conf.*, Mar. 2021, pp. 2494–2498.

Mengdao Xing (Fellow, IEEE) received the B.S. and Ph.D. degrees in electronic engineering from Xidian University, Xi'an, Shaanxi, China, in 1997 and 2002, respectively.

He is currently a Professor with the National Laboratory of Radar Signal Processing, Xidian University. He is the Dean with the Academy of Advanced Interdisciplinary Research Department, Xidian University. He has written or cowritten more than 200 refereed scientific journal articles. He has also authored or coauthored two books about SAR signal processing. The total citation times of his research are greater than 10 000 (H-index 50). He was a Most Cited Chinese Researchers by Elsevier. He has achieved more than 50 authorized China patents. His research has been supported by various funding programs, such as National Science Fund for Distinguished Young Scholars. His research interests are synthetic aperture radar (SAR), SAR interferometry, inversed SAR, sparse signal processing, and microwave remote sensing.

Dr. Xing has held several Special Issues on IEEE GRSM and JSTARS. He is currently the Associate Editor for radar remote sensing of the IEEE TRANSACTIONS ON GEOSCIENCE AND REMOTE SENSING and the Editor-in-Chief of the MDPI Sensors
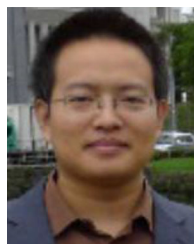
Guang-Cai Sun (Senior Member, IEEE) received the Master's degree in communications engineering from the Xi'an University of Posts and Telecommunications, Xi'an, China, in 2006, and the Ph.D. degree in signal and information processing from Xidian University, Xi'an, in 2012.

He is currently an Associate Professor with the National Laboratory of Radar Signal Processing, and also with the Collaborative Innovation Center of Information Sensing and Understanding, Xidian University. He has authored or coauthored 1 book and authored more than 50 articles. His research interests include imaging of several SAR modes, moving target detection and imaging.

Zhihao Wang (Student Member, IEEE) was born in Anhui, China, in 1995. He received the B.S. degree in electronic information engineering in 2017 from Xidian University, Xi'an, China, where he is currently working toward the Ph.D. degree in signal processing with the National Laboratory of Radar Signal Processing.

His research interests include synthetic aperture radar ground moving target indication, spaceborne early warning radar system design, and signal processing method.

Yongliang Wang (Member, IEEE) received the Ph.D. degree in electrical engineering from Xidian University, Xi'an, China, in 1994.

From 1994 to 1996, he was a Post-Doctoral Fellow with the Department of Electronic Engineering, Tsinghua University, Beijing, China. He has been a Full Professor since 1996, and he was the Director of the Key Research Laboratory with Wuhan Radar Academy, Wuhan, China, from 1997 to 2005. He has authored or coauthored three books and more than 200 papers. His research interests include radar systems, space–time adaptive processing, and array signal processing.

Dr. Wang is a Member of the Chinese Academy of Sciences and a fellow of the Chinese Institute of Electronics. He was a recipient of the China Postdoctoral Award in 2001 and the Outstanding Young Teachers Award of the Ministry of Education, China, in 2001

Shuangxi Zhang (Member, IEEE) was born in Fujian, China, in 1984. He received the B.S. degree in technique of measuring control and instrument engineering in 2008 from Xidian University, Xi'an, China, where he received the Ph.D. degree in signal processing from the National Key Laboratory of Radar Signal Processing in 2014.

He was a Research Fellow with the National University of Singapore , Singapore, from 2014 to 2016. He is currently an Associate Professor with the School of Electronics and Information, Northwestern Polytechnical University, Xi'an, China. He is the Organizer and the Session Chairs of Synthetic Aperture Radar Techniques and Applications-Part1/2 and -Part2/2 in ACES-China 2017, Suzhou. His research interests include SAR imaging, clutter suppression, SAR interference suppression, array signal processing, electromagnetic scattering, etc.

Jixiang Xiang (Student Member, IEEE) was born in Anyang, Henan, China, in 1994. He received the B.S. degree in communication engineering from the University of Electronic Science and Technology of China, Chengdu, China, in 2017. He is currently working toward the Ph.D. degree in signal processing with the National Laboratory of Radar Signal Processing, Xidian University, Xi'an, China.

His research interests include multichannel synthetic aperture radar (SAR) signal processing, and SAR/ground moving target indicator.